The search for new treatment strategies for malignant pleural mesothelioma

Schunselaar, L.M.

Chapter 2

Chemical Profiling of Primary Mesothelioma Cultures Defines Subtypes with Different Expression Profiles and Clinical Responses.

Laurel M. Schunselaar*, Josine M.M.F. Quispel-Janssen*, Yongsoo Kim, Costantine Alifrangis, Wilbert Zwart, Paul Baas and Jacques Neefjes
*equal contribution
Clin Cancer Res. 2018 Apr; 24(7):1761-1770

Abstract

Purpose: Finding new treatment options for patients with malignant pleural mesothelioma is challenging due to the rarity and heterogeneity of this cancer type. The absence of druggable targets further complicates the development of new therapies. Current treatment options are therefore limited and prognosis remains poor.

Experimental design: We performed drug screening on primary mesothelioma cultures to guide treatment decisions of corresponding patients that were progressive after first- or second-line treatment.

Results: We observed a high concordance between in vitro results and clinical outcomes. We defined three subgroups responding differently to the anticancer drugs tested. In addition, gene expression profiling yielded distinct signatures that segregated the differently responding subgroups. These genes signatures involved various pathways, most prominently the fibroblast growth factor pathway.

Conclusions: Our primary mesothelioma culture system has proved to be suitable to test novel drugs. Chemical profiling of primary mesothelioma cultures allows personalizing treatment for a group of patients with a rare tumor type, where clinical trials are notoriously difficult. This personalized treatment strategy is expected to improve the poor prospects of mesothelioma patients.

Keywords

Mesothelioma, clinical responses, genetic profile, FGFR, personalized treatment

Translational relevance

Mesothelioma or asbestos cancer is a tumor with a poor prognosis. Three mesothelioma subtypes have been defined based on morphology, and no effective treatment is available. Here, we describe a system allowing the culture of primary mesothelioma cells for drug testing and genetic analyses. On the basis of drug sensitivities, we define three new mesothelioma subtypes with a concomitant different gene expression profile, including FGF pathway. Translating the results of the primary cultures to the treatment of a small set of patients correctly predicted clinical responses. Chemical profiling of patients with mesothelioma allows identification of subgroups separated by the feature most relevant to patients; drug responses. The corresponding genetic analysis identifies the FGF pathway for targeting in a defined mesothelioma subgroups.

Introduction

Malignant pleural mesothelioma (MPM) is a rare but aggressive tumor arising from mesothelial cells in the pleural cavity. It usually presents with pain or dyspnea, caused by pleural fluid or shrinkage of the hemithorax [1]. Palliative chemotherapy consisting of a platin and antifolate combination is considered standard of care and gives a modest survival advantage of around 3 months [2]. Further systemic treatment can be offered to fit patients, but thus far, studies in second-line failed to detect a survival benefit. Response rates in different second-line therapies range between 0% and 20% [3], which urges the need for more effective treatments.

Using genetic profiling to define drivers in cancer amendable to targeting by small molecular drugs has been successful in other types of tumors. MPM, however, has only a few mutations and none of these present as a likely target for therapy. Most genetic mutations found in MPM are loss of tumor suppressor genes, like CDKN2A, NF2 and BAP1, rather than activation of oncogenes [4]. The absence of druggable molecular targets in MPM hinders the development of more dedicated and effective therapies [5-9].

Based on histology, three types of mesothelioma are recognized: an epithelioid, a sarcomatoid, and a biphasic or mixed type [10]. Epithelioid mesothelioma comprises the largest group and has a better outcome than the sarcomatoid and mixed type. Regarding response to treatment, epithelioid mesothelioma is a heterogeneous disease. To increase the effectivity of current therapies, it is vital to find ways to more accurately profile this group of patients for personalized treatment and new therapeutic options.

Long-established cell lines are commonly used for in vitro drug screens to select compounds

for further clinical development [11]. However, their resemblance to primary tumors is questionable because cells change pheno- and genotypically during their adaptation to tissue culture conditions [12-15]. This can have a profound influence on their responses to anticancer drugs [16, 17]. The use of cell lines in drug development programs did not yield any active drugs for patients with mesothelioma. One example is the VANTAGE-014 trial, which was based on positive results from established cell lines [18]. This study exemplifies the difficulty of conducting clinical trials in a rare disease like mesothelioma [19](12). In this placebo-controlled trial that evaluated the HDAC-inhibitor vorinostat in second or third line, the time to accrue 661 patients with mesothelioma from 90 international centers was 6 years. Unfortunately, there was no clinical benefit from treatment with vorinostat in this very large study [20]. This trial stresses the need for in vitro drug testing conditions that reflect genuine mesothelioma tumors more accurately. Primary mesothelioma cultures may provide a valuable model for personalized drug selection for patients with mesothelioma because they recapitulate the original tumor far more accurately than long-established MPM cell lines [21, 22].

We established a method of profiling primary mesothelioma cultures with commonly used anticancer drugs and validated the results in corresponding patients. We distinguished three groups, not by means of genetic parameters, but based on the drug response patterns, which are ultimately more relevant to the patient. We found that the three “chemical” profiles were associated with three distinct gene expression profiles relating to the FGFR pathway. Indeed, FGFR inhibition blocked proliferation of primary mesothelioma cultures, providing proof-of-concept of chemical profiling as a method to reveal novel sensitivities to targeted agents.

Materials and Methods

Patients

All patients provided written informed consent for the use and storage of pleural fluid, tumor biopsies, and germ line DNA. Separate informed consent was obtained to use the information from the drug screens for making treatment decisions. The study was conducted in accordance with the Declaration of Helsinki and approved by Netherlands Cancer Institute review board. Diagnosis was determined on available tumor biopsies and confirmed by the Dutch Mesothelioma Panel, a national expertise panel of certified pathologists who evaluate all patient samples suspected of mesothelioma.

Culture method

Short-term primary mesothelioma cultures were generated by isolating tumor cells from pleural fluid. Within half an hour after drainage, the pleural fluid was centrifuged at 1,500

rpm for 5 minutes at room temperature (RT). When the cell pellet was highly contaminated with erythrocytes, it was incubated with erythrocyte lysis buffer (containing 150 mmol/L NH_4Cl, 10 mmol/L potassium bicarbonate and 0.2 mmol/L EDTA) for 10 minutes at RT. Cells were resuspended in Dulbecco's Modified Eagle Medium (DMEM, Gibco) supplemented with penicillin/streptomycin and 8% fetal calf serum. The cells were seeded in T75 flasks at a quantity of 10 x 10^6, 15 x 10^6 or 20 x 10^6 cells and incubated at 37°C at 5% CO_2. Medium was refreshed depending on metabolic activity of the cells, usually twice a week. Cells were cultured for a maximum period of 4 weeks.

Comparative genome hybridization (CGH)

To ensure that our cultures consisted mainly of tumor cells, we performed CGH on a number of cultures. CGH was performed as described by Schouten and colleagues [23]. Tumor DNA was labeled with Cy3, and female pooled reference DNA (G1521, Promega) was labeled with Cy5 using the ENZO labeling kit for BAC arrays (ENZ-42670, ENZO Life Sciences). Unincorporated nucleotides were removed with the Qiagen MinElute PCR Purification Kit (28004, Qiagen). Subsequently, tumor and reference DNA were pooled and pelleted using an Eppendorf Concentrator (5301, Eppendorf). The pellets were resuspended in hybridization mix (NimbleGen Hybridization Kit, Roche Nimblegen) and the sample loaded on the array. Hybridization was at 42°C for 40 to 72 hours (Maui Hybridization System, BioMicro Systems). Slides were washed three times (Roche NimbleGen Wash Buffer Kit) and scanned at 2 µm double pass using an Agilent High Resolution Microarray Scanner (Scanner model: G2505C, Agilent). The resulting image files were further analyzed using NimbleScan software (Roche Nimblegen). Grids were aligned on the picture manually and per channel pair files generated. The Nimblescan DNACopy algorithm was applied at default settings and the unaveraged DNAcopy text files were used for further analyses.

Drug screens

Drug screens were performed in biological duplicate after 1 and 2 weeks of culture. Seven single agents (cisplatin, carboplatin, oxaliplatin, vinorelbine, gemcitabine, pemetrexed and doxorubicin) and five combinations (cisplatin + pemetrexed, cisplatin + gemcitabine, carboplatin + pemetrexed, oxaliplatin + gemcitabine and oxaliplatin + vinorelbine) were used. Cells were seeded in a flat bottom 96-wells plate at a density of 5,000 cells/well. After overnight incubation, chemotherapeutics in a concentration range of 50 µmol/L to 5 nmol/L were added in technical triplicates. After 72 hours of incubation with the drugs, the cytotoxicity was measured with a metabolic activity assay (Cell Titer blue G8081, Promenga). Fluorescent readout was performed with the Envision Multilabel Reader (Perkin Elmer).

Interpretation dose-response curves

Classification of cultures in three groups. The classification of cultures in three groups was

based on results from all drugs and drug combinations screened. For three concentrations (10 nmol/L, 1 µmol/L, and 50 µmol/L), cell survival cutoff was determined. Cell survival cutoff for a drug concentration of 10 nmol/L was set at ≥90% cell survival, for 1 µmol/L at ≥70%, and for 50 µmol/L at ≥50%. For each concentration, the number of drugs above the cutoff value was counted. A culture was defined as nonresponsive when for all three concentrations, five or more drugs were above the cell survival cutoff value. A culture was defined as an intermediate responder when for one or two concentrations, five or more drugs were above the cell survival cutoff value. When for all concentrations, less than five drugs were above the cell survival cutoff value, the culture was classified as a responder.
In vitro response prediction. An in vitro response prediction was made for each drug or drug combination individually. The in vitro response was correlated to the clinical response defined by RECIST modified for mesothelioma, thereby identifying patients with progressive disease, stable disease, and partial response. A test set of dose-response curves was used to determine cutoff points for area under the curve (AUC) values to predict clinical responses. Very low or very high drug concentrations were not expected to be clinically relevant. Therefore, the AUC was determined in a concentration range of 50 to 5,000 nmol/L (GraphPad Prism). An AUC level of less than 1,485 predicted a partial response. An AUC level higher than 2,970 predicted progressive disease. All AUC levels between these numbers predicted stable disease.

RNA isolation

Total RNA was extracted using TRIzol reagent (15596-018, Ambion life technologies) according to the manufacturer's protocol. Typically, 1 mL of TRIzol reagent was used per 1×10^6 cells. The total RNA pellet was air dried for 8 minutes, dissolved in an appropriate volume of nuclease-free water (AM9937, Ambion life technologies) and quantified using Nanodrop UV-VIS Spectrophotometer. Total RNA was further purified using the RNeasy MinElute Cleanup Kit (74204, Qiagen) according to the manufacturer's instructions. Quality and quantity of the total RNA was assessed by the 2100 Bioanalyzer using a Nano chip (Agilent). Total RNA samples having RIN >8 were subjected to library generation.

RNA sequencing

Strand-specific libraries were generated using the TruSeq Stranded mRNA sample preparation kit (Illumina Inc., San Diego, RS-122-2101/2) according to the manufacturer's instructions (Illumina, Part # 15031047 Rev. E). The libraries were analyzed on a 2100 Bioanalyzer using a 7500 chip (Agilent), diluted and pooled equimolar into a 10 nmol/L multiplexed sequencing pool and stored at -20°C. The libraries were sequenced with 65-bp paired end reads on a HiSeq2500 using V4 chemistry (Illumina Inc.).

Gene expression analysis

The raw sequencing data were aligned to a human reference genome (build hg38) using tophat 2.0, followed by measuring gene expression using our own protocol based on htseq count (Icount). Normalized count-per million (CPM) was measured using library sizes corrected with Trimmed mean of M-values (TMM) normalization with edgeR package [24]. For differential expressed gene (DEG) identification, we used voom transformation [25] followed by empirical Bayes method with limma r package. Then, DEGs were identified as the genes with P values less than 0.005 and log2 fold changes larger than 2. The voom-transformed log-CPM of DEGs was used in principal component analysis (PCA). For heatmap generation voom-transformed log-CPM of DEGs was standardized by mean centering and scaling with standard deviation. Genes were ordered based on hierarchical clustering with Pearson correlation as a similarity measure and ward linkage. ID number and corresponding fold changes of DEGs were uploaded in ingenuity pathway analysis (IPA; Qiagen Bioinformatics). Analysis was performed with 224 mapped IDs.

Stability assessment of differential gene expression analysis

To assess the reliability of DEGs, we performed differential expression analysis with leaving out each of the responders and nonresponders. The P values and rankings of DEGs that were obtained with this analysis were used in the down-stream analysis. Further, for each of the held-out experiments, we obtained DEGs using same P values and fold-change cutoffs. For each of the DEG lists, hierarchical clustering analysis was performed, after which consensus of the clustering was obtained.

Results

Profiling and characterization of primary mesothelioma cultures

Between February 2012 and July 2016, 155 pleural fluids from 102 patients with a confirmed histological diagnosis of mesothelioma were collected for early passage primary cultures. Eighty-nine patients (87%) were male, the mean age was 67 years and most patients had an epithelial subtype, similar to the conventional distribution of mesothelioma subtypes. Forty-one patients were chemotherapy naïve at the time of cell isolation, and 61 patients had received one or more lines of treatment (Supplementary Table S1A). Figure 1A shows a flow chart of the pleural fluid pipeline depicting in vitro drug testing and subsequent clinical testing in patients. Eighty-one of the 155 isolations were suitable for further culture and drug screening, resulting in a take rate of 52%. These 81 isolations were derived from 57 patients. We failed to perform a drug screen for 45 patients. Patients' characteristics for both groups are given in Supplementary Table S1B and S1C. There was no significant difference between the two groups for age (P=0.05), prior lines of treatment (P=0.54), or histology (P=0.42). There was a significant difference in gender (P=0.03), however the number of female patients was too low to make conclusions about any effect of gender on success rate.

Failure was mainly due to too low tumor cell count isolated from the pleural fluid. The time between isolation of pleural fluid and the start of the first drug screen was generally 1 week. A biological duplicate screen was performed in the following week (Fig. 1B).

Because cultures may change over time, we assessed the stability of our cultures using CGH. While mesothelioma is generally characterized by very few mutations, they frequently show loss of the gene CDKN2A, located at the p16 locus on chromosome 9 [26-28]. This can be detected by CGH. There was no deletion of the p16 locus detected in samples of two patients. In the pleural fluid of three other patients, deletion of the p16 locus was detected in the first culture passages. At later passages, this deletion could not be detected anymore in two of the three patients. Because deletions cannot be repaired spontaneously, this suggests overgrowth of reactive mesothelial cells coisolated with the mesothelioma cells (Supplementary Fig. S2). These experiments validated the isolation and culture of primary mesothelioma cells and showed that drug screens should be performed during the first 3 weeks after isolation from patients, before overgrowth of other cells could be expected.

Chemical profiling identifies three mesothelioma subgroups

Drug screening was performed on 81 different primary cultures with compounds selected on the basis of their current or historical use as treatment of patients with mesothelioma [2, 29-33]. Cisplatin, carboplatin, oxaliplatin, gemcitabine, vinorelbine, pemetrexed and doxorubicin have been tested as single agent and/or in combination. The different cultures showed marked differences in the dose-response profiles. This allowed clustering of the primary cultures in three different groups: so called “responders”, “nonresponders”, and “intermediate responders” (see Materials and Methods). The clustering is based on all drugs and drug combinations screened. We defined a “responder” as a culture responding to most of the chemotherapeutics screened (Fig. 2A; supplementary Fig. S3A). We defined a “non-responder” as a culture failing to respond to more than five of the drugs screened (Fig. 2B and supplementary Fig. S3B). An “intermediate responder” responded to some of the drugs, but not to all of them and visually did not fit in one of the other two categories (Fig. 2C; supplementary Fig. S3C). From the 81 cultures, six cultures classified as “responder”, 27 as “nonresponder” and 48 as “intermediate responders”. Thirty-one drug screens were performed on chemo-naïve cells. Fifty drug screens were performed on cells from patients that received one or more lines of treatments. The clustering in the three groups was not significant different for cells isolated from patients that had or had not received prior treatment (P=0.72; supplementary Table S4A). These data suggested that primary mesothelioma cultures allow subdivision of tumors based on drug sensitivity without significant effects of earlier treatments of the corresponding patients.

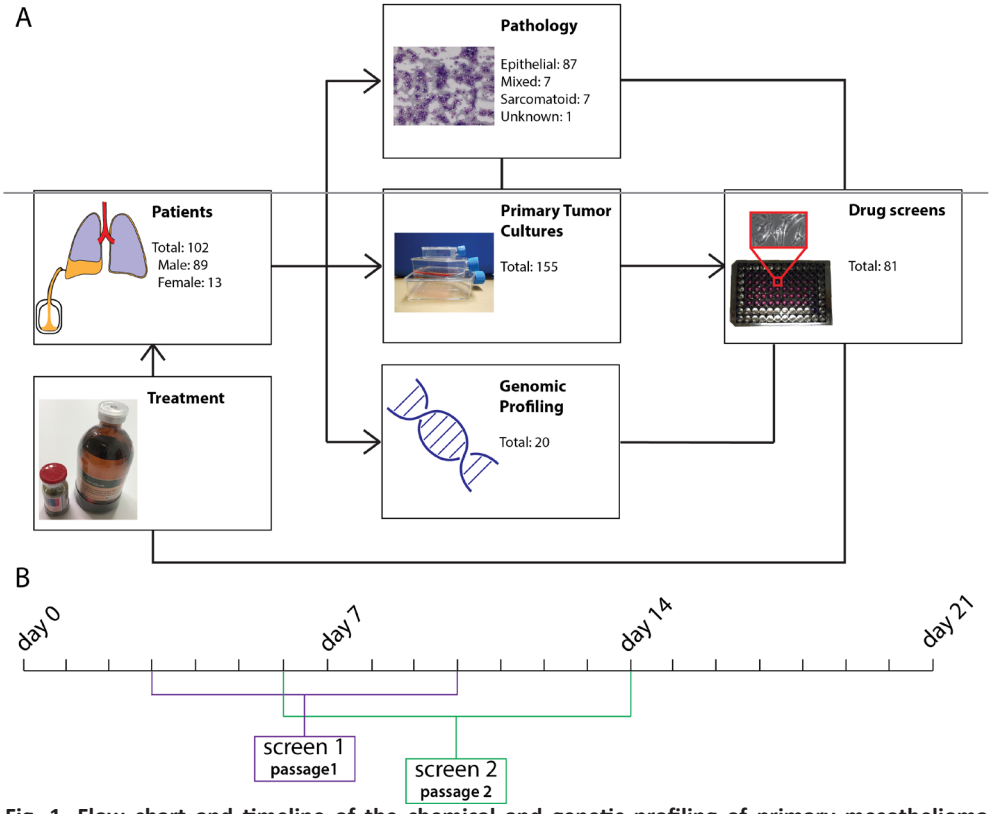

Fig. 1. Flow chart and timeline of the chemical and genetic profiling of primary mesothelioma cultures. A) Flow chart of the pleural fluid pipeline. Pleural fluid was extracted from 102 patients diagnosed with mesothelioma. The cultures were diagnosed with pathology and primary cultures were made. Twenty primary tumor cultures were genetically profiled. Eighty-one cultures were suitable for drug screening. The results from 11 drug screens were used in patient treatment. **B)** Timeline of drug screens using primary mesothelioma cultures. The first screen was started within 10 days after isolation (day 0), the biological duplicate screen was performed within one week after the first screen. The drug screening assays took five days and primary cultures were analyzed within three weeks after cell isolation from the pleural fluid

Transcriptomic analyses reveal distinct genomic subclasses through chemical profiles

Between primary mesothelioma cultures, divergent responses to chemotherapeutic intervention were observed. To test whether there was a genomic basis for these three groups identified by chemical profiling, we performed RNA-seq on 20 primary mesothelioma samples, taken immediately after isolation and representing four “responder” samples, nine “nonresponder” samples, and seven samples from the “intermediate” group. We first identified a set of DEGs between responders and nonresponders with P values less than 0.005 and log2 fold changes larger than 2 (see Material and Methods). A total of 133 genes were

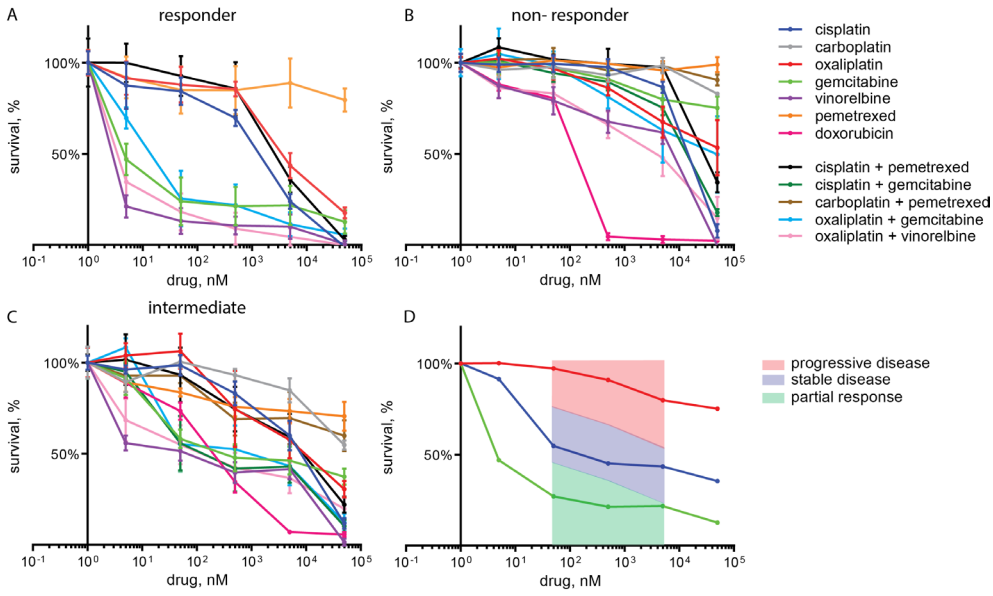

Fig. 2. Dose response curves for various drugs depicted for the differently responding subgroups. A-C) Dose-response curves of a responder, a non-responder and an intermediate responder are shown, as indicated. Drug screens were performed on chemo-naïve cells. Survival (mean ±SD) is shown in relation to increasing concentrations of single agents and combinations, as indicated. **D)** Dose response curves for the drug gemcitabine screened in 3 different patients, a responder (green), an intermediate responder (blue) and a non-responder (red). Boxes indicate the AUC from which progressive disease (red), stable disease (blue) and partial response (green) is predicted. The AUC surface is pictured in the trend of the gemcitabine curves.

Fig. 3. Gene expression profiling of the differently responding mesothelioma subgroups. A) Heatmap showing 285 genes that are differentially expressed between 'responders' and 'non-responders'. Green bars depict genes that are downregulated, while red bars depict upregulated genes in 'non-responders'. The gene expression profile of the intermediate group is different from the expression profile of 'responders' and 'non-responders'. The list of genes is shown in Supplemental table. 2. **B)** Principal Component Analysis separates responders (red) from 'non-responders' (green). The intermediate group (black) locates between these groups. **C)** Ingenuity pathway analysis illustrating the most significant network containing 23 DEGs between 'responders' and 'non-responders'. Green: upregulated, red: downregulated DEGs in non-responders. **D)** Boxplot depicting gene expression of FGF9 and interaction partners FGFR1 and FGFR3 in 'responders' (red), 'non-responders' (green) and 'intermediate responders' (black). The level of gene expression is indicated on the y-axis. Boxplot shows mean expression level with 75th (top) and 25th (bottom) percentile value. Whiskers indicate range of values. **E)** Dose-response curves of two non-responder cultures and reference cell lines NCI-H28 and H2810, treated with increasing concentrations of FGFR inhibitor PD-173074. Cell viability is measured.

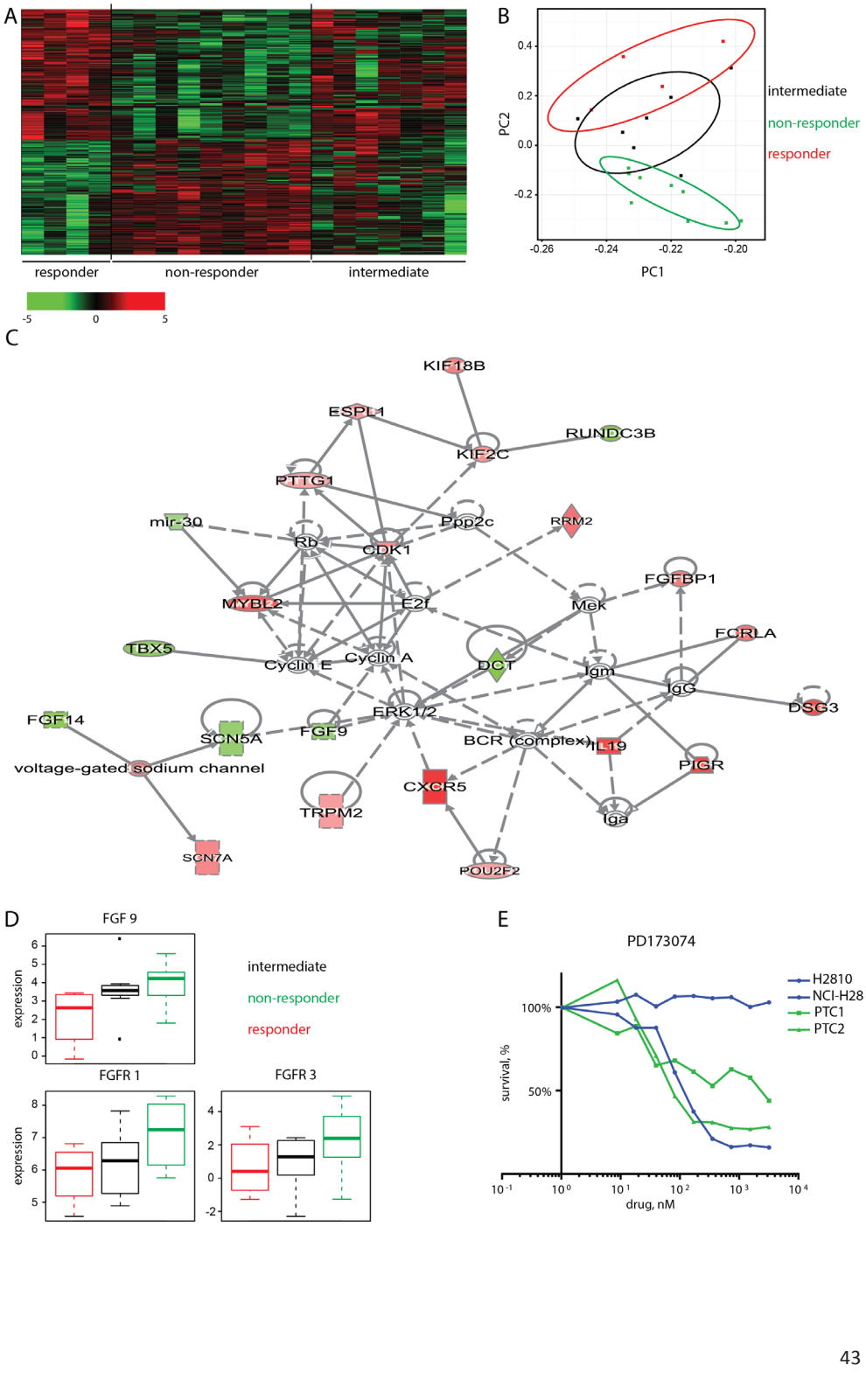
A
responder
non-responder
intermediate
-5
0
5
B
PC2
PC1
0.4
0.2
0.0
-0.2
-0.26
-0.24
-0.22
-0.20
intermediate
non-responder
responder
C
KIF18B
ESPL1
RUNDC3B
KIF2C
PTTG1
mir-30
Rb
Ppp2c
RRM2
CDK1
FGFBP1
MYBL2
E2f
Mek
FCRLA
TBX5
Cyclin E
Cyclin A
DCT
Igm
IgG
DSG3
FGF14
SCN5A
FGF9
ERK1/2
BCR (complex)
IL19
PIGR
voltage-gated sodium channel
CXCR5
TRPM2
Iga
SCN7A
POU2F2
D
FGF 9
expression
intermediate
non-responder
responder
FGFR 1
FGFR 3
expression
E
PD173074
H2810
NCI-H28
PTC1
PTC2
100%
50%
survival, %
drug, nM

downregulated, and 152 genes were upregulated in the “responder” group compared with the “nonresponder” group (supplementary Table S5). In differential gene expression analysis with leave-one-out cross validation, we confirmed that the 285 DEGs were consistently highly ranked and the cutoffs (P<0.005 and log2 fold changes >2) provided genes that stably separated patients by response (supplementary Fig. S6). The “intermediate” group shows a signature that differs from both “responders” and “nonresponders”, also genetically defining it as a separate group (Fig. 3A). We observed the same trend in PCA on expression levels of DEGs (Fig. 3B; Materials and Methods). IPA on DEGs revealed 10 networks containing at least 7 DEGs. The top network with 23 DEGs contained the fibroblast growth factor (FGF) pathway (Fig. 3C). FGF9 was significantly upregulated in the nonresponder group (Fig. 3D). Because this pathway has been described previously in MPM [34], we analyzed gene expression of the preferred receptors for FGF9: FGFR3 and FGFR1. Gene expression of these receptors was also upregulated in the nonresponder group (Fig. 3D). The paired-end RNA-sequencing analysis did not reveal mutated expressed genes.

To test the relevance of the various components of the FGF pathway, primary mesothelioma cultures were exposed to compound PD-173074, an FGFR inhibitor with a high affinity for FGFR3 and FGFR1.

Two “nonresponder” primary mesothelioma cultures were sensitive to the FGFR-inhibitor (Fig. 3E). In mesothelioma cell lines, we also found a statistically significant correlation between elevated FGF9 mRNA expression and IC50 to PD173074 (P=0.0117). These experiments show that chemical profiling of primary mesothelioma cultures allows identification of subgroups that are characterized by different expression profiles. In addition, new targets for treatment of mesothelioma subgroups can be identified, as is illustrated here for the FGF pathway.

Clinical implication of in vitro drug screens

To study the correlation between in vitro drug screens and clinical outcome, we quantified drug sensitivity by calculating the AUC values of dose-response curves. The AUC was determined in a concentration range between 50 and 5,000 nmol/L. Lower or higher concentrations were not expected to be clinically relevant. In vitro response was determined for each drug or drug combination and was classified as the clinical responses: partial response, stable disease or progressive disease. Figure 2D illustrates dose-response curves for the drug gemcitabine in three different patients. The boxes indicate the AUC in which progressive disease, stable disease and partial response were predicted. We treated ten patients that were progressive after first- or second-line treatment, with the drug that was most effective based on the in vitro drug screen, that was performed on the patient’s primary mesothelioma cells (Table 1). Patient 1 was a 61-year-old woman with an epithelial-

type mesothelioma. Her frontline treatment consisted of the standard first-line combination of cisplatin and pemetrexed, which was followed by a surgical procedure consisting of a pleurectomy/decortication. Upon progression, the in vitro drug screen demonstrated oxaliplatin and vinorelbine as the most effective compounds and we predicted a partial response (Fig. 4A, patient 1). She was treated accordingly resulting in a partial response, as is shown in Fig. 4B. The second patient, a 52-year-old male with epithelial mesothelioma, was treated with cisplatin and pemetrexed, followed by a pleurectomy/decortication. Progression occurred 7 months after completion of his first-line therapy. The combination of oxaliplatin and gemcitabine was the most effective one and stable disease was predicted (Fig 4A, patient 2), which was indeed observed after clinical treatment with these drugs (Fig. 4B). Patient 3, a 36-year-old female patient with a mixed type of mesothelioma, had disease progression 4 months after her initial treatment with cisplatin, pemetrexed, and a pleurectomy/decortication. The in vitro drug screen showed a "nonresponder" profile and progressive disease was to be expected from treatment (Fig. 4A, patient 3). She was treated with consecutive courses of the best combination observed (carboplatin/gemcitabine and oxaliplatin/vinorelbine) but experienced disease progression after two courses of each combination (Fig. 4B) and died shortly thereafter. In vitro drug screen results and CT scans before and after treatment of patient 4 to 10 are depicted in Supplementary Fig. S7. For patient 8 to 10, in vitro response prediction correlated with the actual patient response. For patient 4, 6, 7, the patient response was better than predicted. Patient 5, a 71-year-old man with epithelial mesothelioma, was treated twice based on his chemosensitivity screen. After front-line treatment with carboplatin and pemetrexed, he was first treated with gemcitabine and later with vinorelbine. The clinical response for both treatments was stable disease. For gemcitabine, this was predicted based on the in vitro screen. For vinorelbine, however, the observed response was not as pronounced as was expected based on in vitro results (Supplementary Fig. S7). For patient 6, vinorelbine was selected as the best option to which oxaliplatin was added. Patient 7, 9, and 10 did not receive the most potent drug based on in vitro drug screen because of contro-indications for treatment with doxorubicin. Due to the patients' history, vinorelbine or a combination with vinorelbine could not be given. From eleven drug screens, seven in vitro response predictions were correct. For the four that were not correctly predicted, the actual clinical response was better in three patients. These results suggest that the in vitro drug screens had added value in predicting actual individual patient responses to selected drugs.

Discussion

Cancer treatment strategies are changing from general therapy regimens to more personalized treatment, often based on the genetic make-up of the tumor. Unfortunately, no druggable driver mutations have been identified in mesothelioma [5, 6, 8, 9, 35]. Therefore,

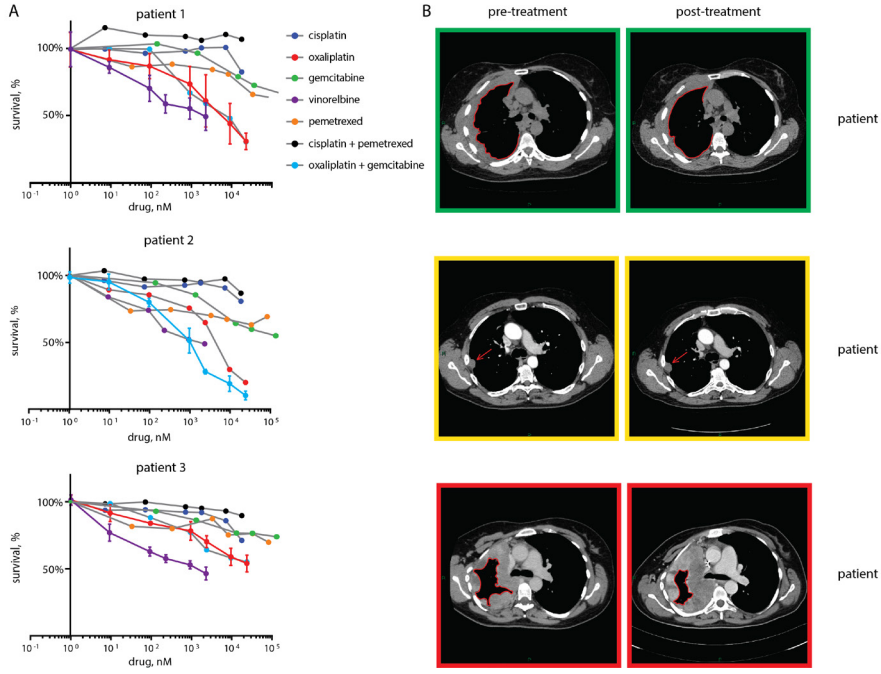

Fig. 4. Dose-response curves and clinical responses of three patients. A) Dose-response curves of primary mesothelioma cells isolated from patients 1-3 and treated with several single agents and combinations of cytotoxic drugs, as indicated. Cell viability measured after 72 hours of drug exposure as a function of increasing concentrations of several drugs and combinations is depicted. **B)** CT-scans of patient 1-3 before and after treatment with the drugs selected based on the in vitro drug screens. Response evaluation was done using modified RECIST for mesothelioma. Colored boxes around CT-scans indicate in vitro response prediction before treatment and the actual response after treatment. Green: partial response, yellow: stable disease, red: progressive disease. Patient 1 was treated with a combination of oxaliplatin and vinorelbine. The tumor rind indicated by the red line is irregular on her pre-treatment scan and is smaller and smoother on her post-treatment scan, indicating a partial response. Patient 2 received a combination of oxaliplatin and gemcitabine. The tumor nodule indicated by the red arrow, remains similar between the scans indicating stable disease. Patient 3 received successively carboplatin/gemcitabin and oxaliplatin/vinorelbine. The grey tumor rind on the pre-treatment scan -encircled by the red line- is larger on the post-treatment scan, which illustrates progressive disease.

Table 1. overview of patients treated based on their in vitro drug screen.

Patient	Gender	Histology	Drug	In vitro predicted response	Patient response
1	F	Epithelial	Oxaliplatin + vinorelbine	PR	PR
2	M	Epithelial	Oxaliplatin + gemcitabine	SD	SD
3	F	Mixed	Oxaliplatin + vinorelbine	PD	PD
4	M	Epithelial	Oxaliplatin + gemcitabine	SD	PR
5-1	M	Epithelial	Gemcitabine	SD	SD
5-2			Vinorelbine	PR	SD
6	M	Epithelial	Oxaliplatin + vinorelbine	PD	SD
7	M	Epithelial	Oxaliplatin + gemcitabine	PD	PR
8	M	Epithelial	Doxorubicine	SD	SD
9	M	Epithelial	Oxaliplatin + gemcitabine	PD	PD
10	M	Epithelial	Oxaliplatin + gemcitabine	SD	SD

F: Female, M: Male, green: PR - partial response, yellow: SD - stable disease, red: PD - progressive disease.

we “chemically” profiled primary mesothelioma cultures with common chemotherapeutic drugs and subsequently treated ten patients with the most effective drug or drug combination. This strategy has previously been successfully applied in lung cancer [36-38], ovarian cancer [39, 40], and breast cancer [41] and showed that in vitro drug responsiveness bears clinically relevant information for patient treatment efficacy.
For the patients treated in this study, we observed considerable overlap between the predicted drug responses in vitro and the corresponding clinical responses. Although the number of patients is too small to make definite conclusions, we present a system that can personalize the treatment of patients with mesothelioma, a heterogeneous disease, with a limited number of patients available for clinical trials and only one registered systemic therapy option.

In addition to predicting the best chemotherapeutic option for an individual patient, we identified “chemical profiles” corresponding to gene signatures that distinguished tumors resistant to most tested therapeutics, from tumors that were largely responsive. A third group with intermediate responses to drugs had an expression profile that was different from the responding and nonresponding group. We expected that drug screens performed on chemo-naïve cells would give a different chemosensitivity profile compared with drug screens performed on pretreated cells. However, no significant differences were detected in the three “chemical profiles” between these groups. This corresponds to results of Mujoomdar and colleagues who described similar results for chemo-naïve and pretreated biopsies treated in vitro with three single agents [42].
The different “chemical profiles” that we identified could not have been identified based on pathology without prior knowledge. In cancer types like prostate and breast cancer, gene expression profiles were successfully used to define subclasses. These were usually retrospectively correlated with prognostic features [43, 44], although one such a profile - the 70-gene signature in breast cancer - has recently been validated on the basis of a prospective study [45]. Our prospectively determined chemical profiles have predictive value, which - from the patients’ perspective - is the most important factor and clinically more relevant than prognostic values.

Of note, there are some limitations to our pipeline. The drug screening system was unable to test pemetrexed. Pemetrexed is an antifolate that inhibits multiple enzymes involved in the formation of nucleotides [46-49]. Pemetrexed activity is competed away by folate [46, 47, 50, 51]. The culture medium used in this system contained folate, probably at supra-physiological levels. Serum also contains a variety of folate, nucleosides, and nucleotides, which is expected to circumvent growth inhibition by pemetrexed [46, 52]. The presence of folate, nucleosides, and nucleotides in the culture system could explain why primary cultures were not sensitive to pemetrexed. Another limitation of the system is that the culture

does not include pharmacokinetics and dynamics of the different drugs. Every cell-based model lacks features of the original tumor like vasculature and tumor micro-environment, which makes it impossible to simulate pharmacokinetics and pharmacodynamics. On logical grounds, our system can also not be used for the testing of the recently introduced classes of immuno-oncology drugs. Our in vitro response prediction method is arbitrary and expanding with more patients would provide data to further define cutoffs for better drug response prediction.

Thus far, we have tested only chemotherapeutics that are commonly used in clinical practice because these allowed validation of the results in patients with mesothelioma. By further expanding the number and classes of compounds in the drug screen, we may not only be able to further characterize the more heterogeneous intermediate group, but also identify more suitable therapeutic options for the nonresponder patient population.
Our model will enable us to select drugs or drug combinations that are more likely to give a response in subgroups of patients. Because mesothelioma is a rare tumor type, such subgroups would probably not have been detected in clinical trials. Preselection of drugs and patients will help to optimize the design and success of clinical trials in this patient group.

We already have one example of a new drug selected on the basis of our method. Based on gene expression profiling, the FGF pathway appeared upregulated in the nonresponder patient population, for whom at this stage no active therapeutic options are available. Deregulated FGF signaling has been linked to cancer pathogenesis [53] and several groups have reported involvement of the FGF signaling cascade in mesothelioma [34, 54]. Because this pathway appeared selectively upregulated in the nonresponder patient population, preselected patients may derive specific benefit from therapeutic intervention using FGFR inhibitors, as we successfully illustrate in our primary cultures (Fig. 3E). Chemical profiling of primary mesothelioma cultures revealed three response groups corresponding to distinct gene signatures involving the FGF signaling cascade. We demonstrated considerable overlap between in vitro and in vivo responses suggesting that our pipeline represents a feasible method to personalize treatment that could ultimately improve the prospects of mesothelioma patients.

Acknowledgements

The authors would like to acknowledge the NKI-AVL Core Facility Mocular Pathology and Biobanking (CFMPB) nd the NKI-AVL Genomic Core Facility for supplying material and lab support. The authors thank Ultan McDermott for this data input. This work was supported by grants from the Dutch Cancer Society (KWF) assigned to P.Baas and J.Neefjes and a gravity program “Institute of Chemical Immunology” assigned to J. Neefjes

References

1. Baas, P., et al., *Malignant pleural mesothelioma: ESMO Clinical Practice Guidelines for diagnosis, treatment and follow-up.* Ann Oncol, 2015. **26 Suppl 5**: p. v31-9.
2. Vogelzang, N.J., et al., *Phase III study of pemetrexed in combination with cisplatin versus cisplatin alone in patients with malignant pleural mesothelioma.* J Clin Oncol, 2003. **21**(14): p. 2636-44.
3. Buikhuisen, W.A., et al., *Second line therapy in malignant pleural mesothelioma: A systematic review.* Lung Cancer, 2015. **89**(3): p. 223-31.
4. Guo, G., et al., *Whole-exome sequencing reveals frequent genetic alterations in BAP1, NF2, CDKN2A, and CUL1 in malignant pleural mesothelioma.* Cancer Res, 2015. **75**(2): p. 264-9.
5. Bonelli, M.A., et al., *New therapeutic strategies for malignant pleural mesothelioma.* Biochem Pharmacol, 2017. **123**: p. 8-18.
6. Cheng, Y.Y., et al., *KCa1.1, a calcium-activated potassium channel subunit alpha 1, is targeted by miR-17-5p and modulates cell migration in malignant pleural mesothelioma.* Mol Cancer, 2016. **15**(1): p. 44.
7. Pignochino, Y., et al., *The combination of sorafenib and everolimus shows antitumor activity in preclinical models of malignant pleural mesothelioma.* BMC Cancer, 2015. **15**: p. 374.
8. Remon, J., et al., *Malignant pleural mesothelioma: new hope in the horizon with novel therapeutic strategies.* Cancer Treat Rev, 2015. **41**(1): p. 27-34.
9. Sekido, Y., *Molecular pathogenesis of malignant mesothelioma.* Carcinogenesis, 2013. **34**(7): p. 1413-9.
10. Churg A, Roggli VL, and G.-S.F.e. al., *Tumours of the pleura: mesothelial tumours.* , in *Pathology and Genetics of Tumours of the Lung, Pleura, Thymus and Heart*, B.E. Travis WD, Muller-Hermelink HK, Harris CC Editor. 2004, IARC, World Health Organization Classification of Tumours . Lyon, France. p. 128–136.
11. Garnett, M.J., et al., *Systematic identification of genomic markers of drug sensitivity in cancer cells.* Nature, 2012. **483**(7391): p. 570-5.
12. Daniel, V.C., et al., *A primary xenograft model of small-cell lung cancer reveals irreversible changes in gene expression imposed by culture in vitro.* Cancer Res, 2009. **69**(8): p. 3364-73.
13. Gillet, J.P., et al., *Redefining the relevance of established cancer cell lines to the study of mechanisms of clinical anti-cancer drug resistance.* Proc Natl Acad Sci U S A, 2011. **108**(46): p. 18708-13.
14. Roschke, A.V., et al., *Karyotypic complexity of the NCI-60 drug-screening panel.* Cancer Res, 2003. **63**(24): p. 8634-47.
15. Tveit, K.M. and A. Pihl, *Do cell lines in vitro reflect the properties of the tumours of origin? A study of lines derived from human melanoma xenografts.* Br J Cancer, 1981. **44**(6): p. 775-86.
16. Das, V., et al., *Pathophysiologically relevant in vitro tumor models for drug screening.* Drug Discov Today, 2015.
17. Eglen, R.M., A. Gilchrist, and T. Reisine, *The use of immortalized cell lines in GPCR screening: the good, bad and ugly.* Comb Chem High Throughput Screen, 2008. **11**(7): p. 560-5.
18. Paik, P.K. and L.M. Krug, *Histone deacetylase inhibitors in malignant pleural mesothelioma: preclinical rationale and clinical trials.* J Thorac Oncol, 2010. **5**(2): p. 275-9.
19. Garassino, M.C. and S. Marsoni, *A lesson from vorinostat in pleural mesothelioma.* Lancet Oncol, 2015. **16**(4): p. 359-60.
20. Krug, L.M., et al., *Vorinostat in patients with advanced malignant pleural mesothelioma who have progressed on previous chemotherapy (VANTAGE-014): a phase 3, double-blind, randomised, placebo-controlled trial.* Lancet Oncol, 2015. **16**(4): p. 447-56.
21. Szulkin, A., et al., *Characterization and drug sensitivity profiling of primary malignant mesothelioma cells from pleural effusions.* BMC Cancer, 2014. **14**: p. 709.
22. Chernova, T., et al., *Molecular profiling reveals primary mesothelioma cell lines recapitulate human disease.* Cell Death Differ, 2016. **23**(7): p. 1152-64.
23. Schouten, P.C., et al., *Platform comparisons for identification of breast cancers with a BRCA-like copy number profile.* Breast Cancer Res Treat, 2013. **139**(2): p. 317-27.
24. Robinson, M.D. and A. Oshlack, *A scaling normalization method for differential expression analysis of RNA-seq data.* Genome Biol, 2010. **11**(3): p. R25.
25. Law, C.W., et al., *voom: Precision weights unlock linear model analysis tools for RNA-seq read counts.* Genome Biol, 2014. **15**(2): p. R29.
26. Musti, M., et al., *Cytogenetic and molecular genetic changes in malignant mesothelioma.* Cancer Genet Cytogenet, 2006. **170**(1): p. 9-15.
27. Illei, P.B., et al., *Homozygous deletion of CDKN2A and codeletion of the methylthioadenosine phosphorylase gene in the majority of pleural mesotheliomas.* Clin Cancer Res, 2003. **9**(6): p. 2108-13.

28. Lopez-Rios, F., et al., *Global gene expression profiling of pleural mesotheliomas: overexpression of aurora kinases and P16/CDKN2A deletion as prognostic factors and critical evaluation of microarray-based prognostic prediction.* Cancer Res, 2006. **66**(6): p. 2970-9.
29. Ceresoli, G.L., et al., *Phase II study of pemetrexed plus carboplatin in malignant pleural mesothelioma.* J Clin Oncol, 2006. **24**(9): p. 1443-8.
30. Ceresoli, G.L. and P.A. Zucali, *Vinca alkaloids in the therapeutic management of malignant pleural mesothelioma.* Cancer Treat Rev, 2015. **41**(10): p. 853-8.
31. Kindler, H.L. and J.P. van Meerbeeck, *The role of gemcitabine in the treatment of malignant mesothelioma.* Semin Oncol, 2002. **29**(1): p. 70-6.
32. Schutte, W., et al., *A multicenter phase II study of gemcitabine and oxaliplatin for malignant pleural mesothelioma.* Clin Lung Cancer, 2003. **4**(5): p. 294-7.
33. Arrieta, O., et al., *First-line chemotherapy with liposomal doxorubicin plus cisplatin for patients with advanced malignant pleural mesothelioma: phase II trial.* Br J Cancer, 2012. **106**(6): p. 1027-32.
34. Schelch, K., et al., *Fibroblast growth factor receptor inhibition is active against mesothelioma and synergizes with radio- and chemotherapy.* Am J Respir Crit Care Med, 2014. **190**(7): p. 763-72.
35. Bueno, R., et al., *Comprehensive genomic analysis of malignant pleural mesothelioma identifies recurrent mutations, gene fusions and splicing alterations.* Nat Genet, 2016. **48**(4): p. 407-16.
36. Cortazar, P., et al., *Survival of patients with limited-stage small cell lung cancer treated with individualized chemotherapy selected by in vitro drug sensitivity testing.* Clin Cancer Res, 1997. **3**(5): p. 741-7.
37. Wilbur, D.W., et al., *Chemotherapy of non-small cell lung carcinoma guided by an in vitro drug resistance assay measuring total tumour cell kill.* Br J Cancer, 1992. **65**(1): p. 27-32.
38. Miyazaki, R., et al., *In Vitro Drug Sensitivity Tests to Predict Molecular Target Drug Responses in Surgically Resected Lung Cancer.* PLoS One, 2016. **11**(4): p. e0152665.
39. Holloway, R.W., et al., *Association between in vitro platinum resistance in the EDR assay and clinical outcomes for ovarian cancer patients.* Gynecol Oncol, 2002. **87**(1): p. 8-16.
40. Matsuo, K., et al., *Prediction of Chemotherapy Response With Platinum and Taxane in the Advanced Stage of Ovarian and Uterine Carcinosarcoma: A Clinical Implication of In vitro Drug Resistance Assay.* Am J Clin Oncol, 2010. **33**(4): p. 358-63.
41. Takamura, Y., et al., *Prediction of chemotherapeutic response by collagen gel droplet embedded culture-drug sensitivity test in human breast cancers.* Int J Cancer, 2002. **98**(3): p. 450-5.
42. Mujoomdar, A.A., et al., *Prevalence of in vitro chemotherapeutic drug resistance in primary malignant pleural mesothelioma: result in a cohort of 203 resection specimens.* J Thorac Cardiovasc Surg, 2010. **140**(2): p. 352-5.
43. Glinsky, G.V., et al., *Gene expression profiling predicts clinical outcome of prostate cancer.* J Clin Invest, 2004. **113**(6): p. 913-23.
44. van 't Veer, L.J., et al., *Gene expression profiling predicts clinical outcome of breast cancer.* Nature, 2002. **415**(6871): p. 530-6.
45. Cardoso, F., et al., *70-Gene Signature as an Aid to Treatment Decisions in Early-Stage Breast Cancer.* N Engl J Med, 2016. **375**(8): p. 717-29.
46. Zhao, R., et al., *Loss of reduced folate carrier function and folate depletion result in enhanced pemetrexed inhibition of purine synthesis.* Clin Cancer Res, 2005. **11**(3): p. 1294-301.
47. Suchy, S.L., et al., *Adaptation of a chemosensitivity assay to accurately assess pemetrexed in ex vivo cultures of lung cancer.* Cancer Biol Ther, 2013. **14**(1): p. 39-44.
48. Calvert, A.H., *Biochemical pharmacology of pemetrexed.* Oncology (Williston Park), 2004. **18**(13 Suppl 8): p. 13-7.
49. Assaraf, Y.G., *Molecular basis of antifolate resistance.* Cancer Metastasis Rev, 2007. **26**(1): p. 153-81.
50. Zhao, R., F. Gao, and I.D. Goldman, *Marked suppression of the activity of some, but not all, antifolate compounds by augmentation of folate cofactor pools within tumor cells.* Biochem Pharmacol, 2001. **61**(7): p. 857-65.
51. Backus, H.H., et al., *Folate depletion increases sensitivity of solid tumor cell lines to 5-fluorouracil and antifolates.* Int J Cancer, 2000. **87**(6): p. 771-8.
52. Lorenzi, M., et al., *Plasma oxypurines in gastric and colorectal cancer.* Biomed Pharmacother, 1990. **44**(8): p. 403-7.
53. Touat, M., et al., *Targeting FGFR Signaling in Cancer.* Clin Cancer Res, 2015. **21**(12): p. 2684-94.
54. Marek, L.A., et al., *Nonamplified FGFR1 Is a Growth Driver in Malignant Pleural Mesothelioma.* Mol Cancer Res, 2014.

Supplementary figures and tables

Table S1 Patient characteristics

A. Characteristics of all patients where cells could be isolated from pleural fluid.

Patients (no.)	102
Male/ female (no./%)	89/ 13 (87%/ 13%)
Mean age (yrs)	67
Prior treatments lines: 0/ 1/ 2/ unknown	41/ 40/ 19/ 2 (40%/ 39%/ 19%/ 2%)
Histology: epithelioid/ sarcomatoid/ mixed/ unknown (no./ %)	87/ 7/ 7/ 1 (85%/ 7%/ 7%/ 1%)

For patients who had multiple cultures at different time points, the number of prior treatment lines was determined at the first successul culture. When we failed to perform a drug screen, the number of prior treatment lines was set at the first culture.

B. Characteristics of patients with a successful drug screen

Patients (no.)	57
Male/ female (no./%)	46/ 11 (81%/ 19%)
Mean age (yrs)	65
Prior treatments lines: 0/ 1/ 2/ unkown (no./%)	26/ 19/ 11/ 1 (46%/ 33%/ 19%/ 2%)
Histology: epithelioid/ sarcomatoid/ mixed/ unknown (no./%)	50/ 4/ 2/ 1 (88%/ 7%/ 4%/ 2%)

C. Characteristics of patients where the drug screen failed.

Patients (no.)	45
Male/ female (no./%)	43/2 (96%/ 4%)
Mean age (yrs)	68
Prior treatments lines: 0/ 1/ 2/ unknown (no./ %)	15/ 21/ 8/ 1 (33%/ 47%/ 18%/ 2%)
Histology: epithelioid/ sarcomatoid/ mixed/ unknown (no/%)	37/ 3/ 5/ 0 (82%/ 7%/ 11%/ 0%)

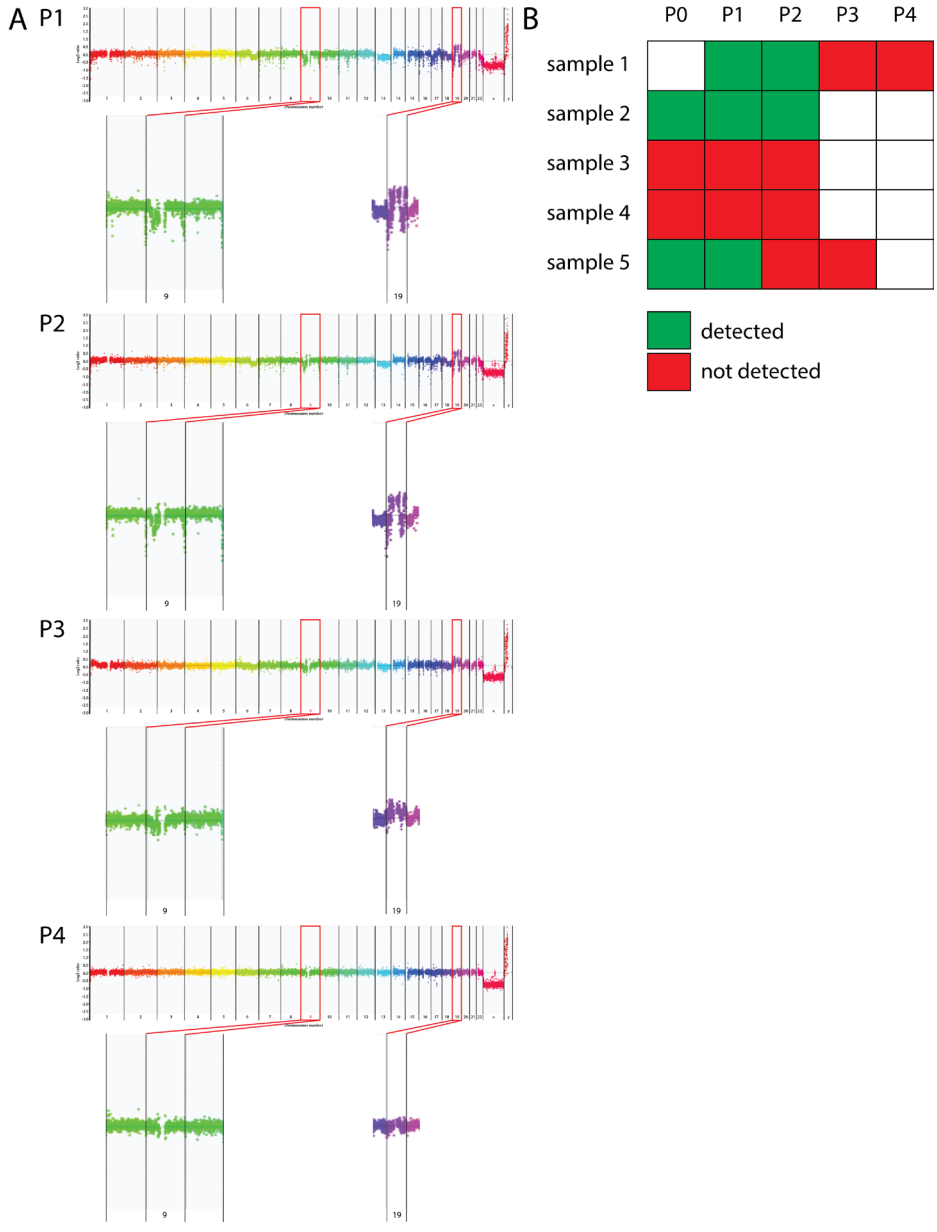

Fig. S2. CGH profiles at different passages of a primary mesothelioma culture. A) The log2 ratio of copy number variations (CNV) is depicted for different chromosomes visualized on the x-axis, each chromosome in a different color. The overall profiles in the first two passages indicate the presence of malignant cells as is illustrated by deletion of the P16 locus on chromosome 9 (shown as an zoom-in in the inset). At higher passages the CNV is normalized indicating overgrowth by normal mesothelial cells. **B)** Overview of CDKN2A deletion for 5 patients. P1: passage 1, P2: passage 2 , P3: passage 3, P4: passage 4. green: detected, red: not detected, white: not assessed. For patient 3 and 4 no deletion could be detected. For patient 1, 2 and 5 the CDKN2A deletion was detected in early passages. At later passages the deletion could not be detected for patient 1 and 5.

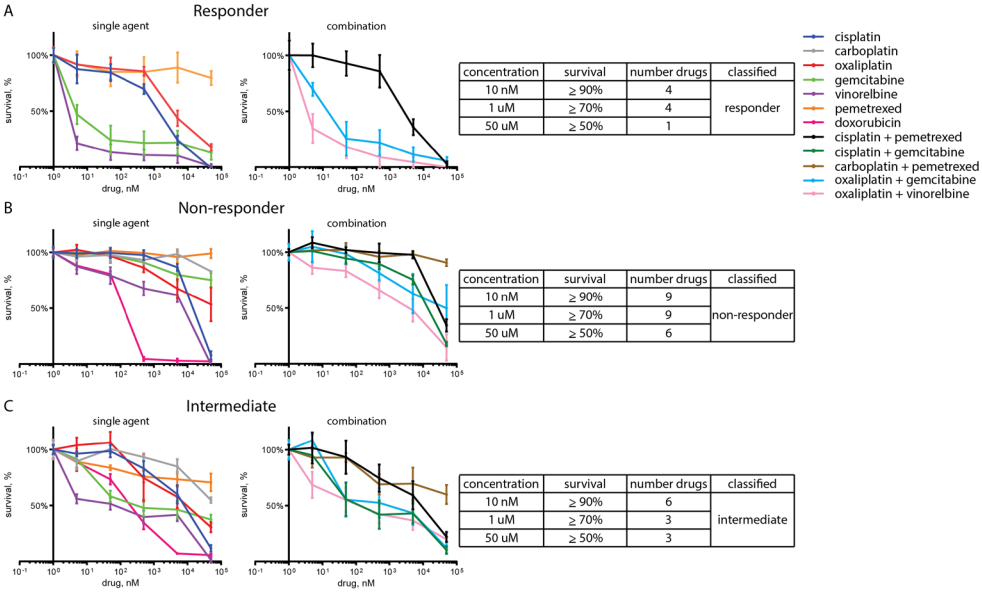

Fig S3. Dose-response curves of single agents and combination depicted for the differently responding subgroups. Dose-response curves of Fig. 2 separated to single agents and combinations are depicted for a responder **A)**, a non responder **B)** and an intermediate responder **C)**. Explanation for the subgroup definition is depicted next to the dose-response curves.

Table S4 Drug screen classification characteristics

	Non-treated		Treated	
	Number	Percentage	Number	Percentage
Drug screens	31	38%	50	62%
Responder	3	10%	3	6%
Intermediate	19	61%	29	58%
Non-responder	9	29%	18	36%

For the characteristics analyzed, there was no significant difference between these two groups (p=0.72)

Table S5. List of differential expressed genes.

Gene ID	Gene Symbol	Gene Name
ENSG00000163995	ABLIM2	actin binding LIM protein family member 2
ENSG00000100312	ACR	acrosin
ENSG00000174837	ADGRE1	adhesion G protein-coupled receptor E1
ENSG00000116771	AGMAT	agmatinase
ENSG00000165695	AK8	adenylate kinase 8
ENSG00000215267	AKR1C7P	aldo-keto reductase family 1 member C7, pseudogene
ENSG00000244301	AOX3P	
ENSG00000006453	BAIAP2L1	BAI1 associated protein 2 like 1
ENSG00000197299	BLM	Bloom syndrome RecQ like helicase
ENSG00000229106	BTBD6P1	BTB domain containing 6 pseudogene 1
ENSG00000221953	C1orf229	chromosome 1 open reading frame 229
ENSG00000128346	C22orf23	chromosome 22 open reading frame 23
ENSG00000225940	C5orf67	chromosome 5 open reading frame 67
ENSG00000118307	CASC1	cancer susceptibility candidate 1
ENSG00000246228	CASC8	cancer susceptibility candidate 8 (non-protein coding)
ENSG00000168491	CCDC110	coiled-coil domain containing 110
ENSG00000274736	CCL23	C-C motif chemokine ligand 23
ENSG00000272398	CD24	CD24 molecule
ENSG00000170312	CDK1	cyclin dependent kinase 1
ENSG00000100162	CENPM	centromere protein M
ENSG00000259430	CERS3-AS1	CERS3 antisense RNA 1
ENSG00000197748	CFAP43	cilia and flagella associated protein 43
ENSG00000172361	CFAP53	cilia and flagella associated protein 53
ENSG00000122966	CIT	citron rho-interacting serine/threonine kinase
ENSG00000144619	CNTN4	contactin 4
ENSG00000273509	CNTNAP3P1	contactin associated protein-like 3 pseudogene 1
ENSG00000124749	COL21A1	collagen type XXI alpha 1 chain
ENSG00000050767	COL23A1	collagen type XXIII alpha 1 chain
ENSG00000158525	CPA5	carboxypeptidase A5
ENSG00000109472	CPE	carboxypeptidase E
ENSG00000150938	CRIM1	cysteine rich transmembrane BMP regulator 1
ENSG00000169429	CXCL8	C-X-C motif chemokine ligand 8
ENSG00000160683	CXCR5	C-X-C motif chemokine receptor 5
ENSG00000080166	DCT	dopachrome tautomerase
ENSG00000165325	DEUP1	deuterosome assembly protein 1
ENSG00000267432	DNAH17-AS1	DNAH17 antisense RNA 1
ENSG00000118997	DNAH7	dynein axonemal heavy chain 7
ENSG00000007174	DNAH9	dynein axonemal heavy chain 9
ENSG00000134757	DSG3	desmoglein 3
ENSG00000198842	DUSP27	dual specificity phosphatase 27 (putative)
ENSG00000165891	E2F7	E2F transcription factor 7
ENSG00000186976	EFCAB6	EF-hand calcium binding domain 6
ENSG00000135373	EHF	ETS homologous factor
ENSG00000188316	ENO4	enolase family member 4
ENSG00000204334	ERICH2	glutamate rich 2
ENSG00000171320	ESCO2	establishment of sister chromatid cohesion N-acetyltransferase 2
ENSG00000264527	ESP33	uncharacterized locus ESP33
ENSG00000135476	ESPL1	extra spindle pole bodies like 1, separase
ENSG00000229007	EXOSC3P1	exosome component 3 pseudogene 1
ENSG00000198780	FAM169A	family with sequence similarity 169 member A
ENSG00000125804	FAM182A	family with sequence similarity 182 member A
ENSG00000175170	FAM182B	family with sequence similarity 182 member B
ENSG00000104059	FAM189A1	family with sequence similarity 189 member A1
ENSG00000269881	FAM234A	family with sequence similarity 234 member A
ENSG00000164616	FBXL21	F-box and leucine rich repeat protein 21 (gene/pseudogene)
ENSG00000132185	FCRLA	Fc receptor like A
ENSG00000181617	FDCSP	follicular dendritic cell secreted protein
ENSG00000230316	FEZF1-AS1	FEZF1 antisense RNA 1
ENSG00000275340	FGD5P1	FYVE, RhoGEF and PH domain containing 5 pseudogene 1
ENSG00000102466	FGF14	fibroblast growth factor 14
ENSG00000102678	FGF9	fibroblast growth factor 9

ENSG00000137440	FGFBP1	fibroblast growth factor binding protein 1
ENSG00000232774	FLJ22447	uncharacterized LOC400221
ENSG00000105255	FSD1	fibronectin type III and SPRY domain containing 1
ENSG00000123689	G0S2	G0/G1 switch 2
ENSG00000197093	GAL3ST4	galactose-3-O-sulfotransferase 4
ENSG00000227135	GCSAML-AS1	GCSAML antisense RNA 1
ENSG00000139278	GLIPR1	GLI pathogenesis related 1
ENSG00000140478	GOLGA6A (includes others)	golgin A6 family member C
ENSG00000170775	GPR37	G protein-coupled receptor 37
ENSG00000138271	GPR87	G protein-coupled receptor 87
ENSG00000167914	GSDMA	gasdermin A
ENSG00000111305	GSG1	germ cell associated 1
ENSG00000075218	GTSE1	G2 and S-phase expressed 1
ENSG00000164588	HCN1	hyperpolarization activated cyclic nucleotide gated potassium channel 1
ENSG00000162639	HENMT1	HEN1 methyltransferase homolog 1
ENSG00000235527	HIPK1-AS1	HIPK1 antisense RNA 1
ENSG00000183598	HIST2H3D	histone cluster 2, H3d
ENSG00000212769	HMGN2P8	high mobility group nucleosomal binding domain 2 pseudogene 8
ENSG00000276975	HYDIN2	HYDIN2, axonemal central pair apparatus protein (pseudogene)
ENSG00000146678	IGFBP1	insulin like growth factor binding protein 1
ENSG00000142224	IL19	interleukin 19
ENSG00000254294	IMPDH1P6	inosine monophosphate dehydrogenase 1 pseudogene 6
ENSG00000123999	INHA	inhibin alpha subunit
ENSG00000183856	IQGAP3	IQ motif containing GTPase activating protein 3
ENSG00000170549	IRX1	iroquois homeobox 1
ENSG00000176049	JAKMIP2	janus kinase and microtubule interacting protein 2
ENSG00000184408	KCND2	potassium voltage-gated channel subfamily D member 2
ENSG00000235262	KDM5C-IT1	KDM5C intronic transcript 1
ENSG00000186185	KIF18B	kinesin family member 18B
ENSG00000116852	KIF21B	kinesin family member 21B
ENSG00000142945	KIF2C	kinesin family member 2C
ENSG00000237649	KIFC1	kinesin family member C1
ENSG00000124743	KLHL31	kelch like family member 31
ENSG00000137812	KNL1	kinetochore scaffold 1
ENSG00000205426	KRT81	keratin 81
ENSG00000233930	KRTAP5-AS1	KRTAP5-1/KRTAP5-2 antisense RNA 1
ENSG00000133317	LGALS12	galectin 12
ENSG00000186152	LILRP1	leukocyte immunoglobulin-like receptor pseudogene 1
ENSG00000170858	LILRP2	leukocyte immunoglobulin-like receptor pseudogene 2
ENSG00000180422	LINC00304	long intergenic non-protein coding RNA 304
ENSG00000214851	LINC00612	long intergenic non-protein coding RNA 612
ENSG00000237945	LINC00649	long intergenic non-protein coding RNA 649
ENSG00000242258	LINC00996	long intergenic non-protein coding RNA 996
ENSG00000271856	LINC01215	long intergenic non-protein coding RNA 1215
ENSG00000249667	LINC01259	long intergenic non-protein coding RNA 1259
ENSG00000249911	LINC01265	long intergenic non-protein coding RNA 1265
ENSG00000251396	LINC01301	long intergenic non-protein coding RNA 1301
ENSG00000227467	LINC01537	long intergenic non-protein coding RNA 1537
ENSG00000079435	LIPE	lipase E, hormone sensitive type
ENSG00000260868	LOC100128905	uncharacterized LOC100128905
ENSG00000234432	LOC100129484	uncharacterized LOC100129484
ENSG00000278909	LOC100130057	uncharacterized LOC100130057
ENSG00000237499	LOC100130476	uncharacterized LOC100130476
ENSG00000257545	LOC100287944	uncharacterized LOC100287944
ENSG00000250365	LOC101927124	uncharacterized LOC101927124
ENSG00000226747	LOC101927196	uncharacterized LOC101927196
ENSG00000250548	LOC101927780	uncharacterized LOC101927780
ENSG00000235834	LOC101928389	uncharacterized LOC101928389
ENSG00000255337	LOC101928424	uncharacterized LOC101928424
ENSG00000261465	LOC102723385	uncharacterized LOC102723385
ENSG00000230010	LOC105372550	uncharacterized LOC105372550

ENSG00000270171	LOC105376689	uncharacterized LOC105376689
ENSG00000233593	LOC105378853	
ENSG00000256050	LOC107984678	uncharacterized LOC107984678
ENSG00000234665	LOC403323	uncharacterized LOC403323
ENSG00000236780	LOC644838	uncharacterized LOC644838
ENSG00000230445	LRRC37A6P	leucine rich repeat containing 37 member A6, pseudogene
ENSG00000240720	LRRD1	leucine rich repeats and death domain containing 1
ENSG00000235448	LURAP1L-AS1	LURAP1L antisense RNA 1
ENSG00000187391	MAGI2	membrane associated guanylate kinase, WW and PDZ domain containing 2
ENSG00000234456	MAGI2-AS3	MAGI2 antisense RNA 3
ENSG00000078018	MAP2	microtubule associated protein 2
ENSG00000008735	MAPK8IP2	mitogen-activated protein kinase 8 interacting protein 2
ENSG00000199094	mir-30	microRNA 30a
ENSG00000208018	mir-645	microRNA 645
ENSG00000263463	MIR378I	microRNA 378i
ENSG00000162006	MSLNL	mesothelin-like
ENSG00000101057	MYBL2	MYB proto-oncogene like 2
ENSG00000250174	MYLK-AS2	MYLK antisense RNA 2
ENSG00000272916	NDST2	N-deacetylase and N-sulfotransferase 2
ENSG00000247809	NR2F2-AS1	NR2F2 antisense RNA 1
ENSG00000167693	NXN	nucleoredoxin
ENSG00000119547	ONECUT2	one cut homeobox 2
ENSG00000099985	OSM	oncostatin M
ENSG00000083454	P2RX5	purinergic receptor P2X 5
ENSG00000257950	P2RX5-TAX1BP3	P2RX5-TAX1BP3 readthrough (NMD candidate)
ENSG00000174740	PABPC5	poly(A) binding protein cytoplasmic 5
ENSG00000107719	PALD1	phosphatase domain containing, paladin 1
ENSG00000231806	PCAT7	prostate cancer associated transcript 7 (non-protein coding)
ENSG00000248383	PCDHAC1	protocadherin alpha subfamily C, 1
ENSG00000262576	PCDHGA4	protocadherin gamma subfamily A, 4
ENSG00000056487	PHF21B	PHD finger protein 21B
ENSG00000164530	PI16	peptidase inhibitor 16
ENSG00000153823	PID1	phosphotyrosine interaction domain containing 1
ENSG00000162896	PIGR	polymeric immunoglobulin receptor
ENSG00000127564	PKMYT1	protein kinase, membrane associated tyrosine/threonine 1
ENSG00000122861	PLAU	plasminogen activator, urokinase
ENSG00000137841	PLCB2	phospholipase C beta 2
ENSG00000136040	PLXNC1	plexin C1
ENSG00000240694	PNMA2	paraneoplastic Ma antigen 2
ENSG00000028277	POU2F2	POU class 2 homeobox 2
ENSG00000184486	POU3F2	POU class 3 homeobox 2
ENSG00000185250	PPIL6	peptidylprolyl isomerase like 6
ENSG00000119938	PPP1R3C	protein phosphatase 1 regulatory subunit 3C
ENSG00000158528	PPP1R9A	protein phosphatase 1 regulatory subunit 9A
ENSG00000068489	PRR11	proline rich 11
ENSG00000112812	PRSS16	protease, serine 16
ENSG00000206549	PRSS50	protease, serine 50
ENSG00000225706	PTPRD-AS1	PTPRD antisense RNA 1
ENSG00000164611	PTTG1	pituitary tumor-transforming 1
ENSG00000076344	RGS11	regulator of G-protein signaling 11
ENSG00000253006	RN7SKP283	
ENSG00000263974	RN7SL121P	RNA, 7SL, cytoplasmic 121, pseudogene
ENSG00000242853	RN7SL749P	
ENSG00000164197	RNF180	ring finger protein 180
ENSG00000251819	RNU6-322P	RNA, U6 small nuclear 322, pseudogene
ENSG00000221340	RNU6ATAC18P	
ENSG00000201558	RNVU1-6	RNA, variant U1 small nuclear 6
ENSG00000213228	RPL12P38	ribosomal protein L12 pseudogene 38
ENSG00000243422	RPL23AP49	ribosomal protein L23a pseudogene 49
ENSG00000171848	RRM2	ribonucleotide reductase regulatory subunit M2
ENSG00000160188	RSPH1	radial spoke head 1 homolog
ENSG00000105784	RUNDC3B	RUN domain containing 3B
ENSG00000160307	S100B	S100 calcium binding protein B
ENSG00000186193	SAPCD2	suppressor APC domain containing 2

ENSG00000183873	SCN5A	sodium voltage-gated channel alpha subunit 5
ENSG00000136546	SCN7A	sodium voltage-gated channel alpha subunit 7
ENSG00000135094	SDS	serine dehydratase
ENSG00000012171	SEMA3B	semaphorin 3B
ENSG00000232352	SEMA3B-AS1	SEMA3B antisense RNA 1 (head to head)
ENSG00000167680	SEMA6B	semaphorin 6B
ENSG00000057149	SERPINB3	serpin family B member 3
ENSG00000206073	SERPINB4	serpin family B member 4
ENSG00000101049	SGK2	SGK2, serine/threonine kinase 2
ENSG00000129946	SHC2	SHC adaptor protein 2
ENSG00000171241	SHCBP1	SHC binding and spindle associated 1
ENSG00000188991	SLC15A5	solute carrier family 15 member 5
ENSG00000103257	SLC7A5	solute carrier family 7 member 5
ENSG00000227258	SMIM2-AS1	SMIM2 antisense RNA 1
ENSG00000206754	SNORD101	small nucleolar RNA, C/D box 101
ENSG00000163071	SPATA18	spermatogenesis associated 18
ENSG00000150628	SPATA4	spermatogenesis associated 4
ENSG00000184005	ST6GALNAC3	ST6 N-acetylgalactosaminide alpha-2,6-sialyltransferase 3
ENSG00000127954	STEAP4	STEAP4 metalloreductase
ENSG00000169302	STK32A	serine/threonine kinase 32A
ENSG00000144834	TAGLN3	transgelin 3
ENSG00000182521	TBPL2	TATA-box binding protein like 2
ENSG00000089225	TBX5	T-box 5
ENSG00000240280	TCAM1P	testicular cell adhesion molecule 1, pseudogene
ENSG00000253304	TMEM200B	transmembrane protein 200B
ENSG00000165685	TMEM52B	transmembrane protein 52B
ENSG00000118503	TNFAIP3	TNF alpha induced protein 3
ENSG00000050730	TNIP3	TNFAIP3 interacting protein 3
ENSG00000188001	TPRG1	tumor protein p63 regulated 1
ENSG00000170893	TRH	thyrotropin releasing hormone
ENSG00000142185	TRPM2	transient receptor potential cation channel subfamily M member 2
ENSG00000157570	TSPAN18	tetraspanin 18
ENSG00000214391	TUBAP2	tubulin alpha pseudogene 2
ENSG00000276043	UHRF1	ubiquitin like with PHD and ring finger domains 1
ENSG00000093134	VNN3	vanin 3
ENSG00000075702	WDR62	WD repeat domain 62
ENSG00000154764	WNT7A	Wnt family member 7A
ENSG00000177752	YIPF7	Yip1 domain family member 7
ENSG00000169064	ZBBX	zinc finger B-box domain containing
ENSG00000221886	ZBED8	zinc finger BED-type containing 8
ENSG00000091656	ZFHX4	zinc finger homeobox 4
ENSG00000229956	ZRANB2-AS2	ZRANB2 antisense RNA 2 (head to head)

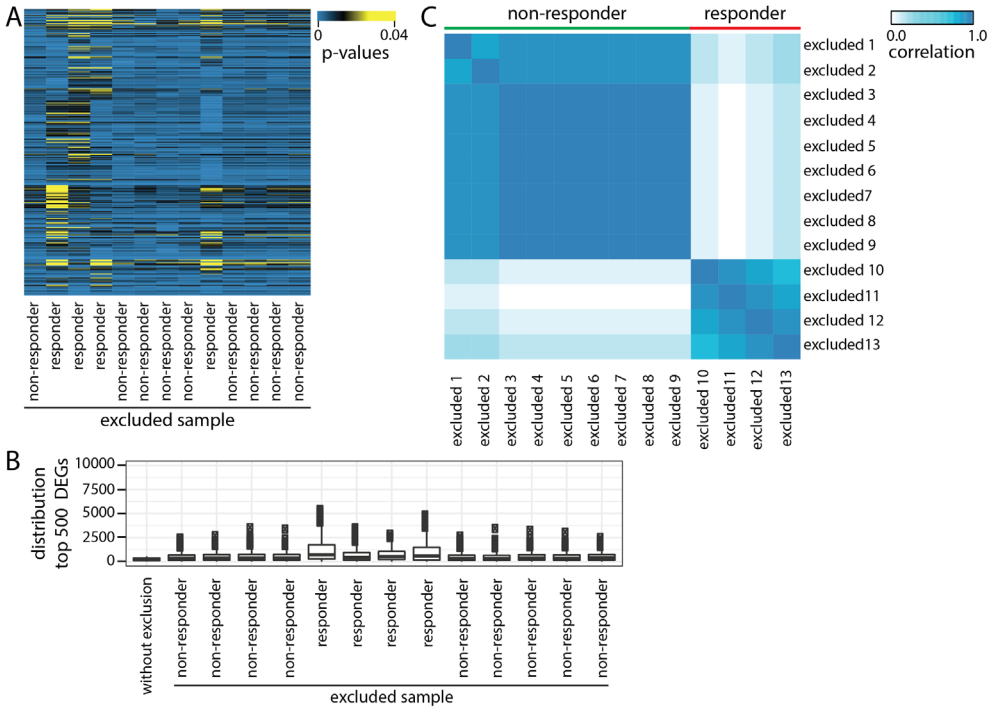

Fig. S6. Stability assessment of differential gene expression analysis. A) Heat map indicating P-values with leave one out cross-validation experiment. Columns are held out samples and rows are held-out genes. **B)** Ranks of DEGs in terms of P-values in the held-out experiment. **C)** Consensus clustering of samples with DEGs obtained from each of the held-out experiment. Color bar indicate patient group.

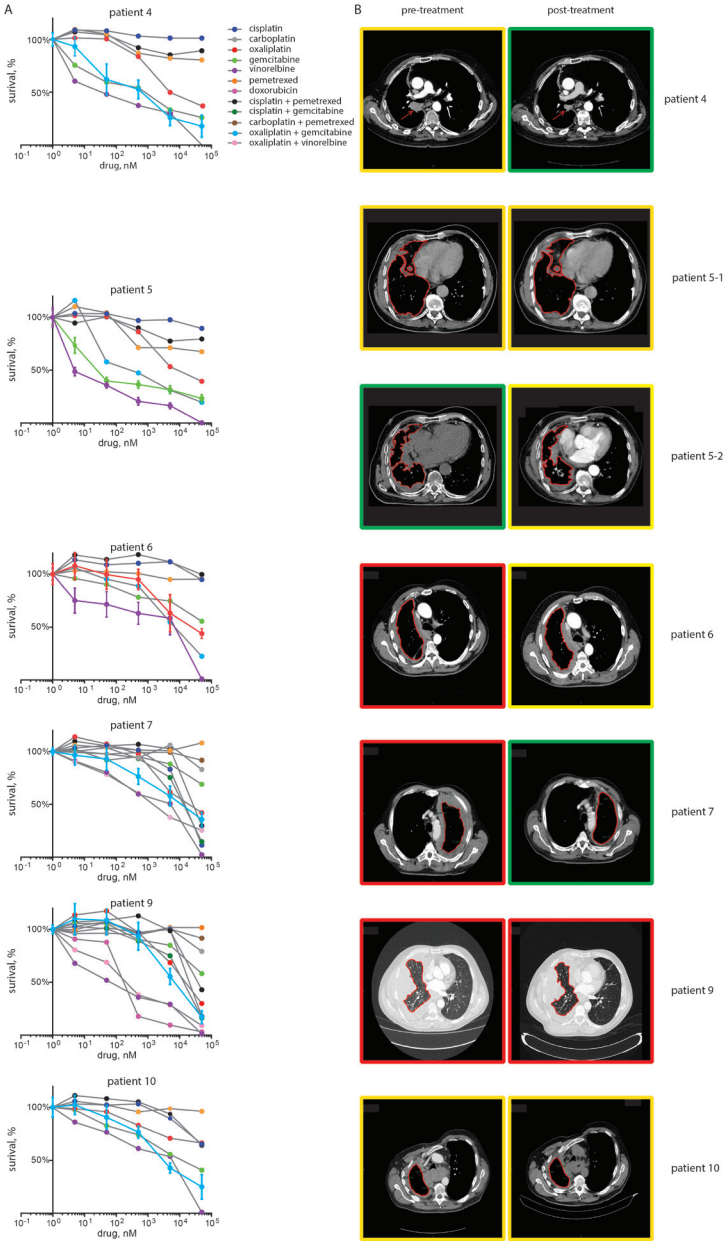

Fig. S7. Dose-response curves and clinical responses. A) Dose-response curves of primary tumor cultures performed for patient 4-7, 9 and 10. The chemotherapeutic agent that was given to the patient is depicted in color the rest of the screened chemotherapeutics is depicted with a gray line and colored dots. **B)** CT-scans of patient 4-7, 9 and 10 before and after treatment with the drugs selected based on the in vitro drug screen. Response evaluation was done using modified RECIST for mesothelioma. Colored boxes around CT-scans indicate in vitro response prediction before treatment and actual response after treatment. Green: partial response, yellow: stable disease, red: progressive disease. Tumor-rinds are indicated by red line.